robotics

MDPI

Article

Cat-Inspired Gaits for a Tilt-Rotor—From Symmetrical to Asymmetrical

Zhe Shen * and Takeshi Tsuchiya

Department of Aeronautics and Astronautics, The University of Tokyo, Tokyo 1138654, Japan; tsuchiya@mail.ecc.u-tokyo.ac.jp

* Correspondence: zheshen@g.ecc.u-tokyo.ac.jp

Abstract: Among the tilt-rotors (quadrotors) developed in recent decades, Ryll's model with eight inputs (four magnitudes of thrusts and four tilting angles) attracted great attention. Typical feedback linearization maneuvers all of the eight inputs with a united control rule to stabilize this tilt-rotor. Instead of assigning the tilting angles by the control rule, the recent research predetermines the tilting angles and leaves the magnitudes of thrusts with the only control signals. These tilting angles are designed to mimic the cat-trot gait while avoiding the singular decoupling matrix in feedback linearization. To complete the discussions of the cat-gait inspired tilt-rotor gaits, this research addresses the analyses on the rest of the common cat gaits, walk, run, transverse gallop, and rotary gallop. It is found that the singular decoupling matrix exists in walk gait, transverse gallop gait, and rotary gallop gait; the decoupling matrix can hardly be guaranteed to be invertible analytically. Further modifications (scaling) are conducted to these three gaits to accommodate the application of feedback linearization; the acceptable attitudes, leading to invertible decoupling matrix, for each scaled gait are evaluated in the roll-pitch diagram. The modified gaits with different periods are then applied to the tilt-rotor in tracking experiments, in which the references are uniform rectilinear motion and uniform circular motion with or without the equipment of the modified attitude-position decoupler. All the experiments are simulated in Simulink, MATLAB. The result shows that these gaits, after modifications, are feasible in tracking references, especially for the cases equipped with the modified attitude-position decoupler.

Keywords: feedback linearization; tilt-rotor; cat gait; gait plan; simulation

Citation: Shen, Z.; Tsuchiya, T. Cat-Inspired Gaits for a Tilt-Rotor—From Symmetrical to Asymmetrical. *Robotics* **2022**, *11*, 60. https://doi.org/10.3390/robotics11030060

Academic Editor: Angelo Cenedese

Received: 23 March 2022
Accepted: 13 May 2022
Published: 13 May 2022

1. Introduction

The tilt-rotor quadrotor [1–4], which is also referred to as the thrust vectoring quadrotor [5,6], is a novel type of quadrotor. Augmented with an additional mechanical structure [7,8], it is able to provide lateral force. Among the designs of the tilt-rotor, Ryll's model, the tilt-rotor with eight inputs, received great attention in the last decade.

Various control methods have been analyzed in stabilizing Ryll's model. These methods include feedback linearization [1], geometric control [9], PID (proportional integral derivative) control [10], backstepping and sliding mode control [11], etc. Among them, the feedback linearization is the first approach [12] proposed in controlling Ryll's model; this method decouples the original nonlinear system to generate the scenario compatible with the linear controller.

However, several unique properties of feedback linearization can hinder the application of this method. One of them is the saturation in feedback linearization [13], which is parallel to the saturation in the geometric control [14]. Also, the state drift phenomenon can be a problem [15]. Another issue is the intensive change in the tilting angles while applying feedback linearization; the resulting changes in the tilting angles can be too large or too intensive. Notice that this intensive change in the tilting angles is not unique in the feedback linearization, e.g., PID [16].

Generally [17], the eight inputs are fully assigned by a united control rule, which makes the number of degrees of freedom less than [12] or equal to [10] the number of inputs. Indeed, these approaches avoid the under-actuated system. Further, the decoupling matrix in this scenario is invertible within the interested attitude region while applying feedback linearization. However, the adverse effect is the intensive change in the tilting angles mentioned beforehand, which may not be desired in application.

Our previous research [18] averts this problem by decreasing the number of inputs of the tilt-rotor. Instead of assigning the tilting angles by the united control rule, a gait plan is applied to the tilting angles beforehand, leaving the magnitudes of thrusts the only actual control inputs. It produces an under-actuated control scenario with the attitude region introducing the singularity in the decoupling matrix. The tilting angles mimicked the cat-trot gait in other research [19] about the tracking problems.

The cat-trot-inspired gait plan for the tilt-rotor guarantees that the decoupling matrix is always invertible during the entire flight, given that the attitude is close to zero, e.g., roll angle and pitch angle are close to zero [19]. The determinant of the relevant decoupling matrix is proved non-zero analytically, assuming that the roll angle and pitch angle are zero.

Unfortunately, the determinant of the decoupling matrix of the gaits analyzed in this paper are not guaranteed to be non-zero without the restrictions on the attitude.

This paper provides novel gaits inspired by the rest of the typical cat gaits, both symmetrical (walk and run) and asymmetrical (transverse gallop and rotary gallop) [20], for the tilt-rotor. The singularity of the decoupling matrix for each of these gaits is analyzed numerically; some gaits are modified by scaling to receive an invertible decoupling matrix before applying feedback linearization. Note that this scaling method is proved to be an effective approach to modify the unqualified gaits, e.g., the gait introducing invertible decoupling matrix only in a small region of the attitude, for a tilt-rotor for the first time.

The degrees of freedom tracked directly are attitude and altitude, e.g., roll, pitch, yaw, and altitude. The rest positions are influenced by manipulating the attitude properly; the modified position-attitude decoupler for the tilt-rotor advanced in the previous research [19] is adopted to track the position.

Two references (uniform rectilinear motion and uniform circular motion) are designed for the tilt-rotor to track in the experiments. Each of the four gaits is applied and analyzed with different periods in the tracking experiment. The result of the position-tracking problem is also compared in the cases with or without advancing the attitude-altitude decoupler. The experiment is simulated in Simulink, MATLAB.

The rest of this paper is structured as follows. Section 2 introduces the dynamics of the tilt-rotor. The controller and the gaits are designed in Section 3. Section 4 analyzes the singularity of the decoupling matrix in each gait and puts forward a gait modification method. Section 5 sets up the references in the tracking problem. The result is demonstrated in Section 6. The conclusions and discussions are addressed in Section 7.

2. Dynamics of the Tilt-Rotor

This section details the dynamics of the tilt-rotor. A comprehensive discussion on it can be referred to in previous studies adopting the same dynamics model [12,18,19].

The model of the tilt-rotor investigated in this study, Figure 1 [18], was initially put forward by Ryll [12].

The frames introduced in the dynamics of this tilt-rotor are the earth frame $\mathcal{F}_E$, body-fixed frame $\mathcal{F}_B$, and four rotor frames $\mathcal{F}_{C_i}(i = 1, 2, 3, 4)$, each of which is fixed on the tilt motor mounted on the end of each arm. Rotor 1 and 3 are assumed to rotate clockwise along Z_{C_1} and Z_{C_3}. Rotor 2 and 4 are assumed to rotate counter-clockwise along Z_{C_2} and Z_{C_4}.

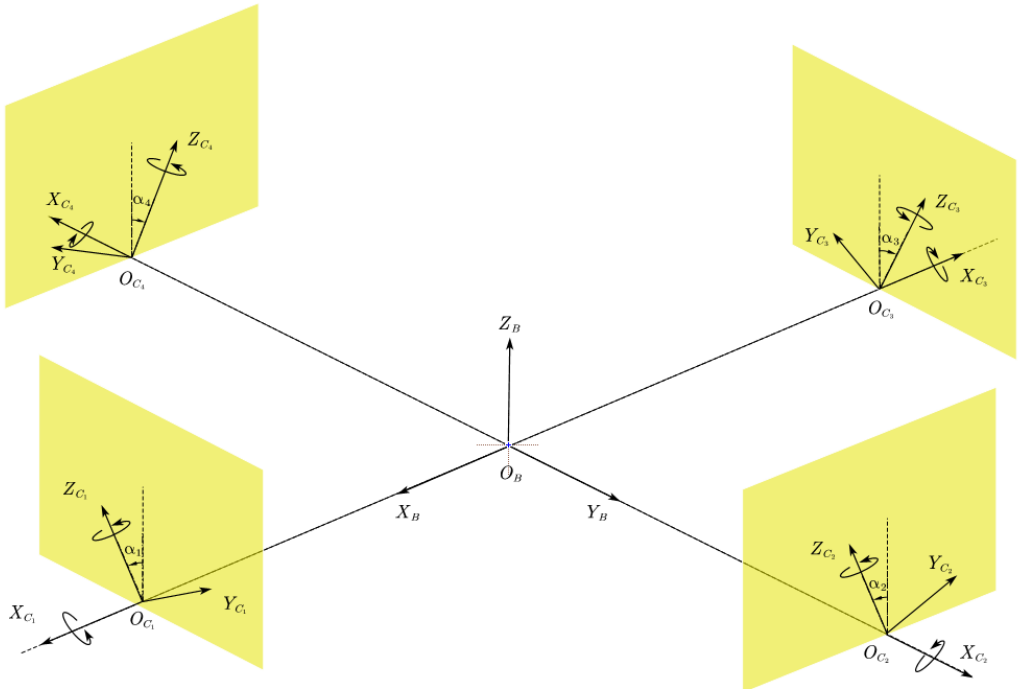

Figure 1. The sketch of a tilt-rotor.

Based on the Newton-Euler formula, the position of the tilt-rotor [18] is given by

$$\ddot{P} = \begin{bmatrix} 0 \\ 0 \\ -g \end{bmatrix} + \frac{1}{m} \cdot {}^{W}R \cdot F(\alpha) \cdot \begin{bmatrix} \varpi_1 \cdot |\varpi_1| \\ \varpi_2 \cdot |\varpi_2| \\ \varpi_3 \cdot |\varpi_3| \\ \varpi_4 \cdot |\varpi_4| \end{bmatrix} \triangleq \begin{bmatrix} 0 \\ 0 \\ -g \end{bmatrix} + \frac{1}{m} \cdot {}^{W}R \cdot F(\alpha) \cdot w \tag{1}$$

where $P = \begin{bmatrix} X & Y & Z \end{bmatrix}^T$ represents the position with respect to $\mathcal{F}_E$, m represents the total mass, g represents the gravitational acceleration, ϖ_i, $(i = 1,2,3,4)$ represents the angular velocity of the propeller ($\varpi_{1,3} < 0$, $\varpi_{2,4} > 0$) with respect to $\mathcal{F}_{C_i} (i = 1,2,3,4)$, $w = [\varpi_1 \cdot |\varpi_1|, \varpi_2 \cdot |\varpi_2|, \varpi_3 \cdot |\varpi_3|, \varpi_4 \cdot |\varpi_4|]^T$, ${}^{W}R$ represents the rotational matrix [21],

$${}^{W}R = \begin{bmatrix} c\theta \cdot c\psi & s\phi \cdot s\theta \cdot c\psi - c\phi \cdot s\psi & c\phi \cdot s\theta \cdot c\psi + s\phi \cdot s\psi \\ c\theta \cdot s\psi & s\phi \cdot s\theta \cdot s\psi + c\phi \cdot c\psi & c\phi \cdot s\theta \cdot s\psi - s\phi \cdot c\psi \\ -s\theta & s\phi \cdot c\theta & c\phi \cdot c\theta \end{bmatrix} \tag{2}$$

where $s\Lambda = \sin(\Lambda)$ and $c\Lambda = \cos(\Lambda)$. ϕ, θ, and ψ are roll angle, pitch angle, and yaw angle, respectively, the tilting angles $\alpha = \begin{bmatrix} \alpha_1 & \alpha_2 & \alpha_3 & \alpha_4 \end{bmatrix}$. The positive directions of the tilting angles are defined in Figure 1. $F(\alpha)$ is given by

$$F(\alpha) = \begin{bmatrix} 0 & K_f \cdot s2 & 0 & -K_f \cdot s4 \\ K_f \cdot s1 & 0 & -K_f \cdot s3 & 0 \\ -K_f \cdot c1 & K_f \cdot c2 & -K_f \cdot c3 & K_f \cdot c4 \end{bmatrix} \tag{3}$$

where $si = \sin(\alpha_i)$, $ci = \cos(\alpha_i)$, and $(i = 1,2,3,4)$. K_f (8.048×10^{-6} N·s^2/rad^2) is the coefficient of the thrust.

The angular velocity of the body with respect to $\mathcal{F}_B$, $\omega_B = \begin{bmatrix} p & q & r \end{bmatrix}^T$, is governed (Newton-Euler formula) by

$$\dot{\omega}_B = {I_B}^{-1} \cdot \tau(\alpha) \cdot w \tag{4}$$

where I_B is the matrix of moments of inertia, K_m (2.423×10^{-7} N·m·s^2/rad^2) is the coefficient of the drag, and L is the length of the arm,

$$\tau(\alpha) = \begin{bmatrix} 0 & L{\cdot}K_f{\cdot}c2 - K_m{\cdot}s2 & 0 & -L{\cdot}K_f{\cdot}c4 + K_m{\cdot}s4 \\ L{\cdot}K_f{\cdot}c1 + K_m{\cdot}s1 & 0 & -L{\cdot}K_f{\cdot}c3 - K_m{\cdot}s3 & 0 \\ L{\cdot}K_f{\cdot}s1 - K_m{\cdot}c1 & -L{\cdot}K_f{\cdot}s2 - K_m{\cdot}c2 & L{\cdot}K_f{\cdot}s3 - K_m{\cdot}c3 & -L{\cdot}K_f{\cdot}s4 - K_m{\cdot}c4 \end{bmatrix}. \quad (5)$$

The relationship [22–24] between the angular velocity of the body, ω_B, and the attitude rotation matrix ($^W R$) is given by

$$^W\dot{R} = {}^W R{\cdot}\hat{\omega}_B \quad (6)$$

where "^" is the hat operation used to produce the skew matrix, $^W\dot{R}$ represents the derivative of rotation matrix.

The parameters of this tilt-rotor are specified as follows: $m = 0.429$ kg, $L = 0.1785$ m, $g = 9.8$ N/kg, $I_B = \mathrm{diag}\left(\left[2.24 \times 10^{-3}, 2.99 \times 10^{-3}, 4.80 \times 10^{-3}\right]\right)$ kg·m^2.

3. Controller Design and Gait Plan

The same control method as in our previous research [18,19] is adopted. This section briefs this controller and introduces animal-inspired gaits analyzed in this study.

3.1. Feedback Linearization and Modified Attitude-Position Decoupler

The degrees of freedom controlled independently in this research are selected as attitude (ϕ, θ, and ψ) and altitude (Z).

Define

$$\begin{bmatrix} y_1 \\ y_2 \\ y_3 \\ y_4 \end{bmatrix} = \begin{bmatrix} \phi \\ \theta \\ \psi \\ Z \end{bmatrix}. \quad (7)$$

Assuming

$$\dot{\alpha}_i \equiv 0, i = 1, 2, 3, 4. \quad (8)$$

we receive

$$\begin{aligned} \begin{bmatrix} \ddot{y}_1 \\ \ddot{y}_2 \\ \ddot{y}_3 \\ \ddot{y}_4 \end{bmatrix} &= \begin{bmatrix} {I_B}^{-1}{\cdot}\tau(\alpha) \\ \begin{bmatrix} 0 & 0 & 1 \end{bmatrix}{\cdot}\frac{K_f}{m}{\cdot}{}^W R{\cdot}F(\alpha){\cdot}2{\cdot}\begin{bmatrix} |\omega_1| & & & \\ & |\omega_2| & & \\ & & |\omega_3| & \\ & & & |\omega_4| \end{bmatrix} \end{bmatrix}^{4\times 4}{\cdot}\begin{bmatrix} \dot{\omega}_1 \\ \dot{\omega}_2 \\ \dot{\omega}_3 \\ \dot{\omega}_4 \end{bmatrix} \\ &+ \begin{bmatrix} 0 & 0 & 1 \end{bmatrix}{\cdot}\frac{K_f}{m}{\cdot}{}^W R{\cdot}\hat{\omega}_B{\cdot}F(\alpha){\cdot}w{\cdot}\begin{bmatrix} 0 \\ 0 \\ 0 \\ 1 \end{bmatrix} \\ &\triangleq \overline{\Delta}{\cdot}\begin{bmatrix} \dot{\omega}_1 \\ \dot{\omega}_2 \\ \dot{\omega}_3 \\ \dot{\omega}_4 \end{bmatrix} + Ma. \end{aligned} \quad (9)$$

where $\overline{\Delta}$ is called the decoupling matrix [25], $\begin{bmatrix} \dot{\omega}_1 & \dot{\omega}_2 & \dot{\omega}_3 & \dot{\omega}_4 \end{bmatrix}^T \triangleq U$ is the new input vector, and Ma are the remaining terms not containing $\dot{\omega}_1$, $\dot{\omega}_2$, $\dot{\omega}_3$, or $\dot{\omega}_4$, which is $\begin{bmatrix} 0 & 0 & 1 \end{bmatrix}{\cdot}K_f/m{\cdot}{}^W R{\cdot}\hat{\omega}_B{\cdot}F(\alpha){\cdot}w{\cdot}[0\,0\,0\,1]^T$.

Finally, design the PD (proportional derivative) controller based on

$$\begin{bmatrix} \dot{\omega}_1 \\ \dot{\omega}_2 \\ \dot{\omega}_3 \\ \dot{\omega}_4 \end{bmatrix} = \overline{\Delta}^{-1} \cdot \left(\begin{bmatrix} \dddot{y}_{1d} \\ \dddot{y}_{2d} \\ \dddot{y}_{3d} \\ \dddot{y}_{4d} \end{bmatrix} - Ma \right). \tag{10}$$

where $\dddot{y}_{id} (i = 1, 2, 3, 4)$ represents the PD controller, which is detailed in Appendix A.

Our previous research [18] approximates the necessary and sufficient condition to receive an invertible decoupling matrix, given non-zero angular velocities in the propellers. That is

$$\begin{array}{l} 4.000 \cdot c1 \cdot c2 \cdot c3 \cdot c4 + 5.592 \cdot (+c1 \cdot c2 \cdot c3 \cdot s4 - c1 \cdot c2 \cdot s3 \cdot c4 + c1 \cdot s2 \cdot c3 \cdot c4 - s1 \cdot c2 \cdot c3 \cdot c4) \\ +0.9716 \cdot (+c1 \cdot c2 \cdot s3 \cdot s4 + c1 \cdot s2 \cdot s3 \cdot c4 + s1 \cdot c2 \cdot c3 \cdot s4 + s1 \cdot s2 \cdot c3 \cdot c4) + 2.000 \\ \cdot (-c1 \cdot s2 \cdot c3 \cdot s4 - s1 \cdot c2 \cdot s3 \cdot c4) + 0.1687 \\ \cdot (-c1 \cdot s2 \cdot s3 \cdot s4 + s1 \cdot c2 \cdot s3 \cdot s4 - s1 \cdot s2 \cdot c3 \cdot s4 + s1 \cdot s2 \cdot s3 \cdot c4) \\ \neq 0. \end{array} \tag{11}$$

Once the gait (combination of the tilting angles) satisfies (11), the decoupling matrix in feedback linearization is asserted to be invertible in our case, given $\phi \approx 0, \theta \approx 0, \psi \approx 0$.

The next question is how to control the remaining degrees of freedom, X and Y in position.

The conventional quadrotor tracks the position by adjusting its attitude based on the conventional attitude-position decoupler [16,24,26]. This decoupler, however, may not be valid for a tilt-rotor. Our previous research [19] deduced the modified attitude-position decoupler for the tilt-rotor,

$$\phi = \frac{1}{g} \cdot \left(\ddot{X} \cdot s\psi - \ddot{Y} \cdot c\psi \right) + \frac{F_Y}{mg}. \tag{12}$$

$$\theta = \frac{1}{g} \cdot \left(\ddot{X} \cdot c\psi + \ddot{Y} \cdot s\psi \right) - \frac{F_X}{mg}. \tag{13}$$

where F_X and F_Y are defined by

$$\begin{bmatrix} F_X \\ F_Y \end{bmatrix} = K_f \cdot \begin{bmatrix} 0 & s2 & 0 & -s4 \\ s1 & 0 & -s3 & 0 \end{bmatrix} \cdot \begin{bmatrix} {I_B}^{-1} \cdot \tau(\alpha) \\ \frac{K_f}{m} \cdot \begin{bmatrix} 0 & 0 & 1 \end{bmatrix} \cdot F(\alpha) \end{bmatrix}^{-1} \cdot \begin{bmatrix} 0 \\ 0 \\ 0 \\ g \end{bmatrix}. \tag{14}$$

One of the comparisons we will make in the tracking result is the simulations equipped with the conventional attitude-position decoupler and with the modified attitude-position decoupler.

3.2. Symmetrical and Asymmetrical Cat-Inspired Gait

The gait for a tilt-rotor is defined as the combination of time-specified tilting angles. Our previous research [19] deployed the cat-trot inspired gait, which leads to the invertible decoupling matrix, satisfying (11).

In this research, several other common cat gaits are discussed before being modified to accommodate (11) and being applied to the tilt-rotor-gait plan.

The cat gaits can be classified as symmetrical gaits and asymmetrical gaits. The footfalls in the former gaits touches the ground at evenly spaced interval of time, which is not the case for the latter gaits [20]. Typical symmetrical gaits include walk, run, and trot. While transverse gallop and rotary gallop are asymmetrical gaits. The target gaits within the scope of this research are walk, run, transverse gallop, and rotary gallop.

These four gaits, given that the period is 1 s, can be approximated (interpolation) in Figures 2–5, respectively. The abscissa represents the time in a period (0 to 1 s). The ordinate represents the relevant tilting angles, α_1, α_2, α_3, and α_4, at the corresponding given time point.

Obviously, the condition (11) may not hold for the gaits designed, leading to a singular decoupling matrix. The problems referring to singularities are discussed in the next section.

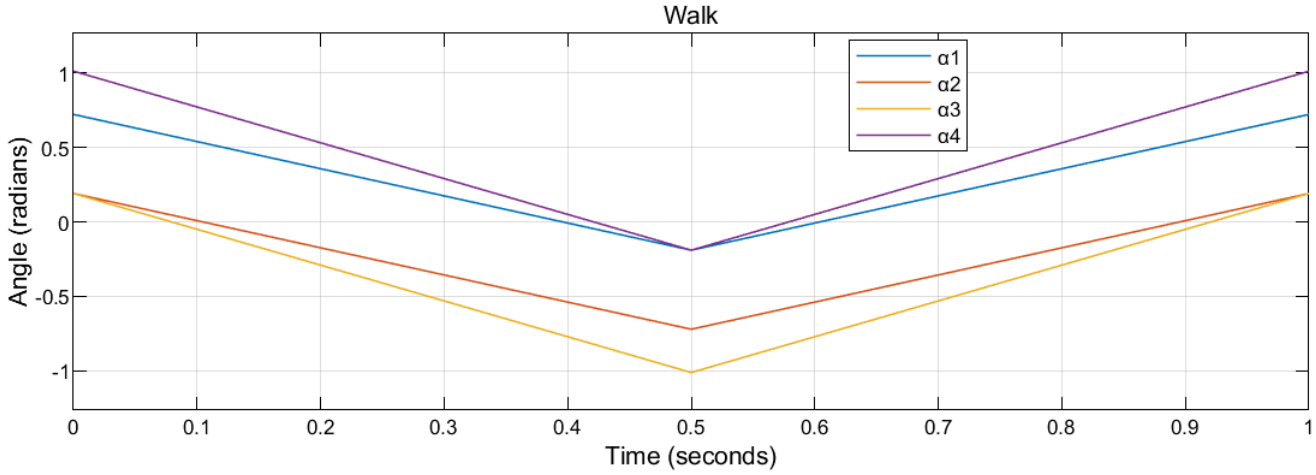

Figure 2. The walk gait of a cat. The period is set as 1 s.

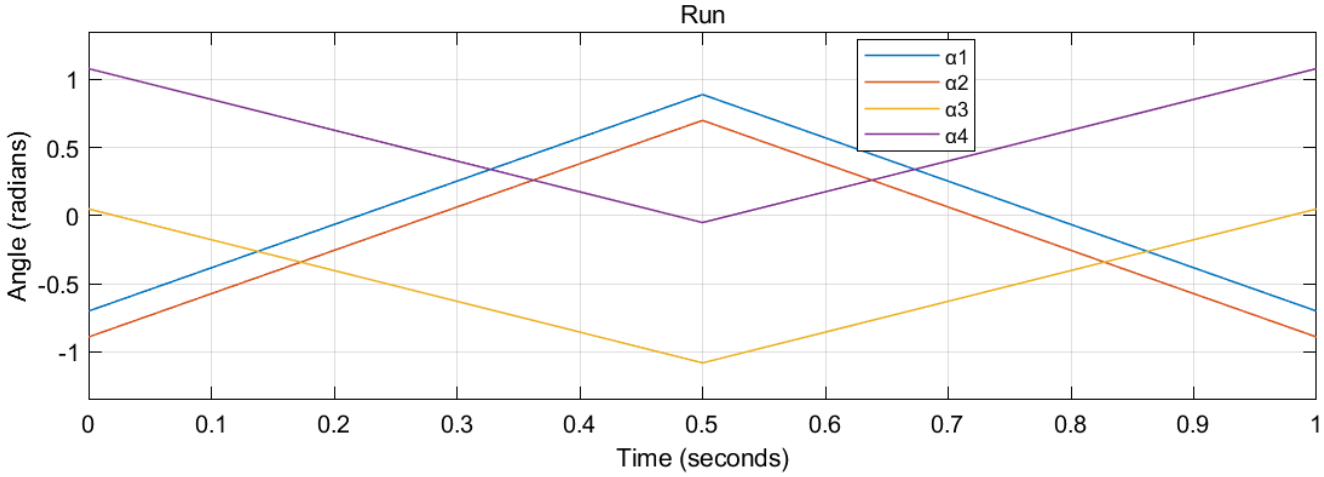

Figure 3. The run gait of a cat. The period is set as 1 s.

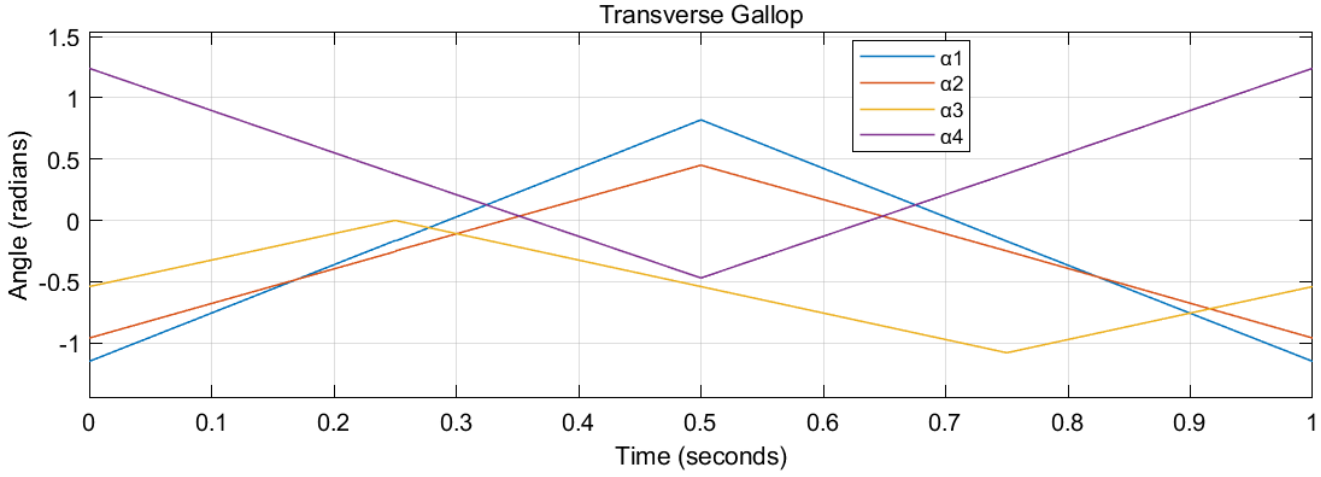

Figure 4. The transverse gallop gait of a cat. The period is set as 1 s.

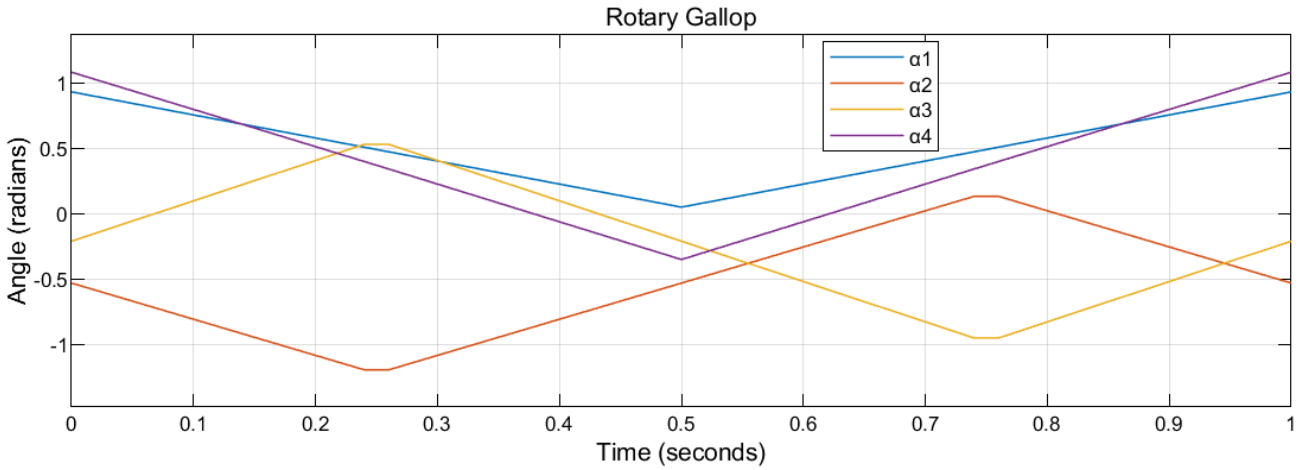

Figure 5. The rotary gallop gait of a cat. The period is set as 1 s.

4. Singular Decoupling Matrix and Gait Modification

The decoupling matrix is required to be invertible while applying feedback linearization. This section discusses the singularity of the decoupling matrix.

The preliminary condition to receive an invertible decoupling matrix is given in (11). However, satisfying (11) does not necessarily mean that the decoupling matrix is invertible.

One may notice that satisfying (11) can also encounter zero angular velocities of the propellers, leading to a singular decoupling matrix. There is other research focusing on the bound-avoidance of the inputs/states [27], which is beyond the scope of this study.

Also, notice that the necessary and sufficient condition in (11) is an approximation at $\phi = 0, \theta = 0$. On the other hand, as explained in our previous research [19], the state $\phi = 0, \theta = 0$ is not a typical equilibrium state. This causes us to visualize the attitudes with the risk of introducing a singular decoupling matrix.

The exact necessary and sufficient condition [18] to receive an invertible decoupling matrix is

$$\begin{aligned}
&1.000{\cdot}c1{\cdot}c2{\cdot}c3{\cdot}s4{\cdot}s\theta - 1.000{\cdot}c1{\cdot}s2{\cdot}c3{\cdot}c4{\cdot}s\theta - 2.880{\cdot}c1{\cdot}c2{\cdot}s3{\cdot}s4{\cdot}s\theta + 2.880{\cdot}c1{\cdot}s2\\
&{\cdot}s3{\cdot}c4{\cdot}s\theta - 2.880{\cdot}s1{\cdot}c2{\cdot}c3{\cdot}s4{\cdot}s\theta + 2.880{\cdot}s1{\cdot}s2{\cdot}c3{\cdot}c4{\cdot}s\theta - 1.000{\cdot}s1{\cdot}c2{\cdot}s3{\cdot}s4{\cdot}s\theta\\
&+1.000{\cdot}s1{\cdot}s2{\cdot}s3{\cdot}c4{\cdot}s\theta + 4.000{\cdot}c1{\cdot}c2{\cdot}c3{\cdot}c4{\cdot}c\phi{\cdot}c\theta + 5.592{\cdot}c1{\cdot}c2{\cdot}c3{\cdot}s4{\cdot}c\phi{\cdot}c\theta\\
&-5.592{\cdot}c1{\cdot}c2{\cdot}s3{\cdot}c4{\cdot}c\phi{\cdot}c\theta + 5.592{\cdot}c1{\cdot}s2{\cdot}c3{\cdot}c4{\cdot}c\phi{\cdot}c\theta - 5.592{\cdot}s1{\cdot}c2{\cdot}c3{\cdot}c4{\cdot}c\phi{\cdot}c\theta\\
&+1.000{\cdot}c1{\cdot}c2{\cdot}s3{\cdot}c4{\cdot}s\phi{\cdot}c\theta + 0.9716{\cdot}c1{\cdot}c2{\cdot}s3{\cdot}s4{\cdot}c\phi{\cdot}c\theta - 2.000{\cdot}c1{\cdot}s2{\cdot}c3{\cdot}s4{\cdot}c\phi{\cdot}c\theta\\
&+0.9716{\cdot}c1{\cdot}s2{\cdot}s3{\cdot}c4{\cdot}c\phi{\cdot}c\theta - 1.000{\cdot}s1{\cdot}c2{\cdot}c3{\cdot}c4{\cdot}s\phi{\cdot}c\theta + 0.9716{\cdot}s1{\cdot}c2{\cdot}c3{\cdot}s4{\cdot}c\phi{\cdot}c\theta\\
&-2.000{\cdot}s1{\cdot}c2{\cdot}s3{\cdot}c4{\cdot}c\phi{\cdot}c\theta + 0.9716{\cdot}s1{\cdot}s2{\cdot}c3{\cdot}c4{\cdot}c\phi{\cdot}c\theta + 2.880{\cdot}c1{\cdot}c2{\cdot}s3{\cdot}s4{\cdot}s\phi{\cdot}c\theta\\
&+2.880{\cdot}c1{\cdot}s2{\cdot}s3{\cdot}c4{\cdot}s\phi{\cdot}c\theta - 0.1687{\cdot}c1{\cdot}s2{\cdot}s3{\cdot}s4{\cdot}c\phi{\cdot}c\theta - 2.880{\cdot}s1{\cdot}c2{\cdot}c3{\cdot}s4{\cdot}s\phi{\cdot}c\theta\\
&+0.1687{\cdot}s1{\cdot}c2{\cdot}s3{\cdot}s4{\cdot}c\phi{\cdot}c\theta - 2.880{\cdot}s1{\cdot}s2{\cdot}c3{\cdot}c4{\cdot}s\phi{\cdot}c\theta - 0.1687{\cdot}s1{\cdot}s2{\cdot}c3{\cdot}s4{\cdot}c\phi{\cdot}c\theta\\
&+0.1687{\cdot}s1{\cdot}s2{\cdot}s3{\cdot}c4{\cdot}c\phi{\cdot}c\theta - 1.000{\cdot}c1{\cdot}s2{\cdot}s3{\cdot}s4{\cdot}s\phi{\cdot}c\theta + 1.000{\cdot}s1{\cdot}s2{\cdot}c3{\cdot}s4{\cdot}s\phi{\cdot}c\theta\\
&\neq 0.
\end{aligned} \tag{15}$$

Once $\alpha_i (i = 1, 2, 3, 4)$ is determined, the unacceptable attitude can be found in $\phi - \theta$ plane by equaling the left side of (15) to 0. The unqualified gaits, leading to the invertible decoupling matrix only in a small attitude region, can be modified by scaling,

$$\alpha_i \leftarrow \frac{\alpha_i}{n}, i = 1, 2, 3, 4, n \geqslant 2, n \in \mathbb{N}. \tag{16}$$

The tilting angles are then scaled by $1/n$ in this modification.

Proposition 1. *There will always be a positive integer n such that the modified gait by scaling by 1/n produces an invertible decoupling matrix.*

Proof of Proposition 1. For a sufficiently large n, we have

$$\lim_{n \to +\infty} \alpha_i = 0. \tag{17}$$

Substituting (17) into the left side of (15) yields

$$4.000 \cdot c\phi \cdot c\theta. \tag{18}$$

which is non-zero, given $\phi \in (-\pi/2, \pi/2), \theta \in (-\pi/2, \pi/2)$, satisfying (15). □

The walk gait, transverse gallop, and rotary gallop gait are scaled by 1/3, respectively, into Figures 6–8. Identical to the previous notations, the abscissa represents the time in a period (0 to 1 s). The ordinate represents the relevant tilting angles, α_1, α_2, α_3, and α_4, at the corresponding given time point.

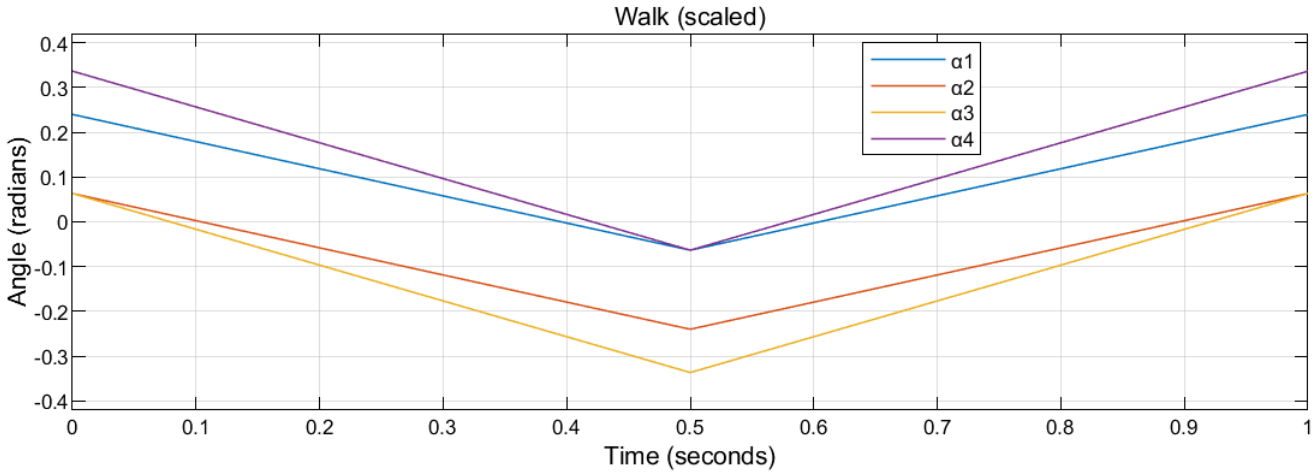

Figure 6. The scaled (1/3) walk gait of a cat. The period is set as 1 s.

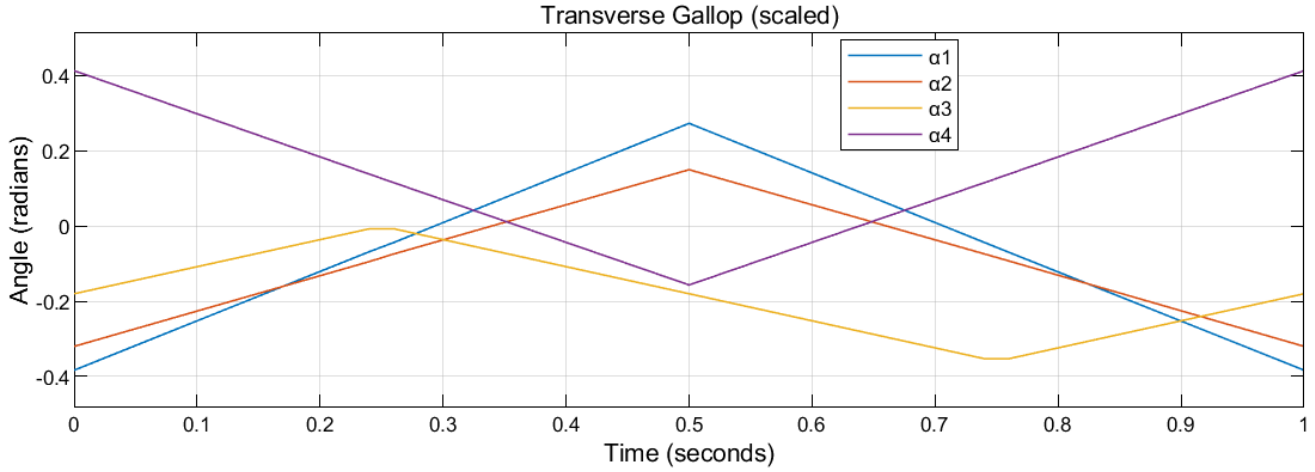

Figure 7. The scaled (1/3) transverse gallop gait of a cat. The period is set as 1 s.

For a given gait, four time-specified tilting angles define the unacceptable attitudes as the attitudes that violate Formula (15); these unacceptable attitudes lead the left side of Formula (15) to zero.

Equaling the left side of Formula (15) to zero, the unacceptable attitudes, ϕ and θ, can be tracked by finding the roots, given a determined gait. The unacceptable attitudes in $\phi - \theta$ plane for different scaled walk gaits are plotted in Figure 9.

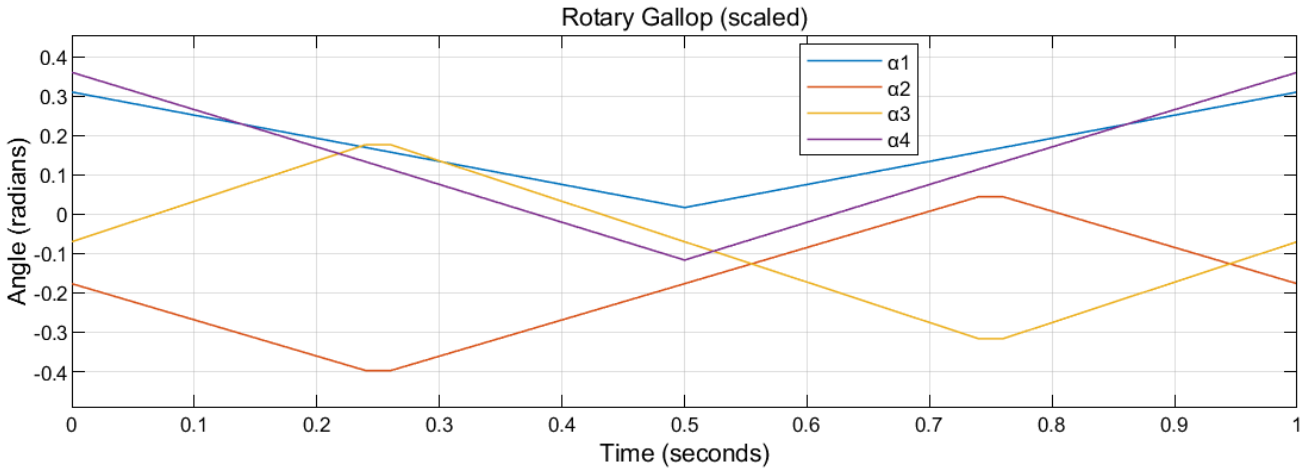

Figure 8. The scaled (1/3) rotary gallop gait of a cat. The period is set as 1 s.

Since the attitudes of most flights are near $(\phi, \theta) = (0, 0)$, we evaluate the quality of a gait by finding the distance between $(\phi, \theta) = (0, 0)$ and the closest curve of the unacceptable attitudes. For a gait receiving a long distance between $(0, 0)$ and the closest curve of the unacceptable attitudes, the tilt-rotor has a large acceptable attitude region. A gait receiving a short distance between $(0, 0)$ and the closest curve of the unacceptable attitudes in the roll-pitch diagram provides a small acceptable attitude region.

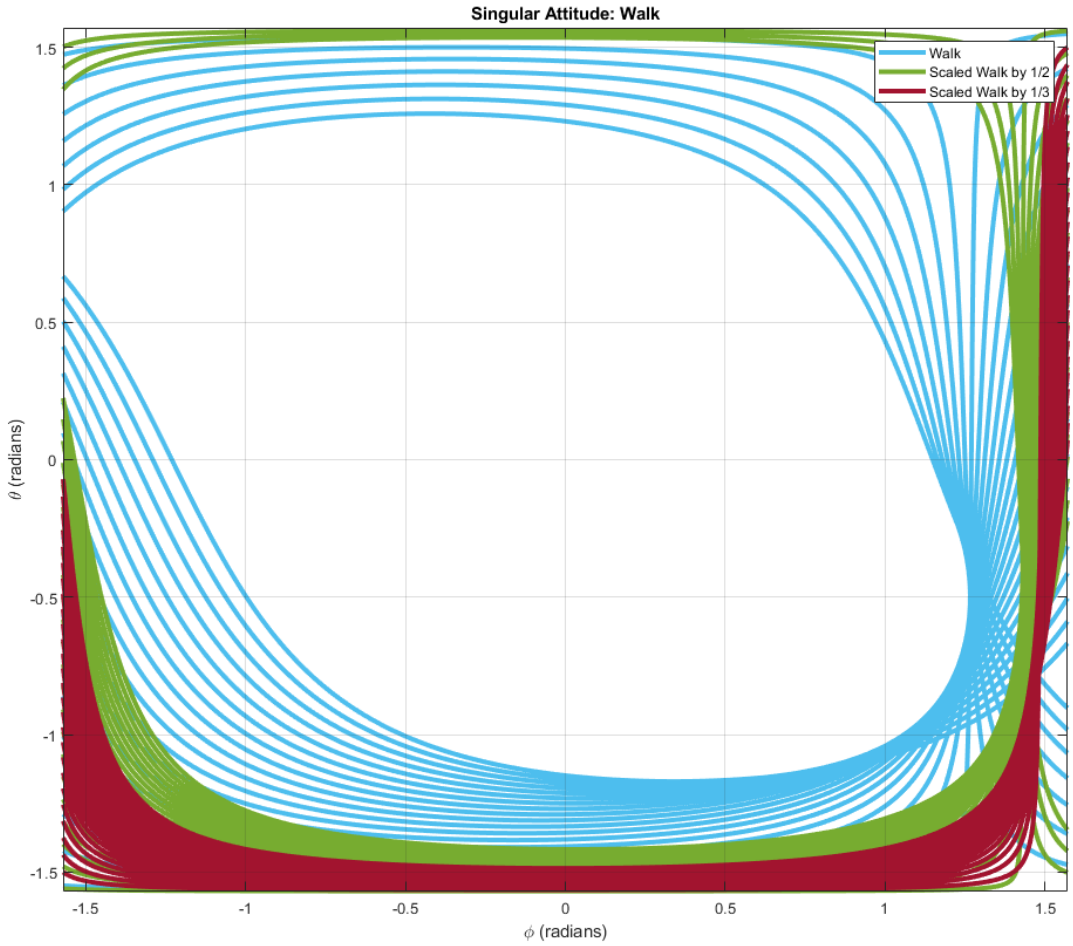

Figure 9. The attitudes introducing the singular decoupling matrix. The blue curve represents the attitudes adopting the walk gait. The green and brown curves represent the attitudes adopting the scaled (1/2 and 1/3, respectively) walk gait.

Thus, a gait with a larger distance between $(0,0)$ and the curve of the unacceptable attitudes is more robust to the attitude; the acceptable attitude region for the tilt-rotor adopting this gait is wider.

It can be found that the acceptable attitude region is enlarging while evenly shrinking the scale of the walk gait. A similar result can also be notably observed in scaled transverse gallop gaits (Figure 10) and scaled rotary gallop gaits (Figure 11).

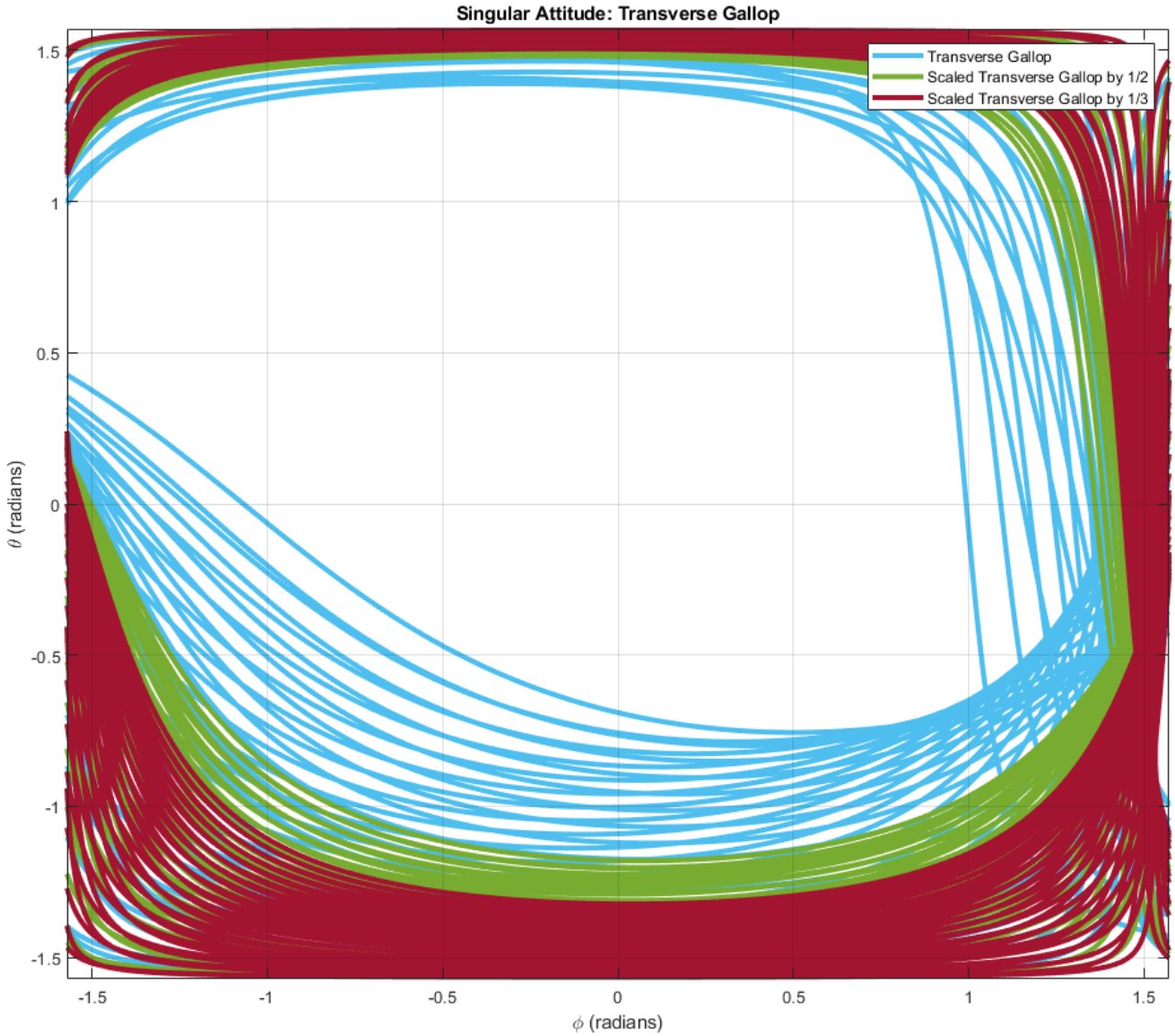

Figure 10. The attitudes introducing the singular decoupling matrix. The blue curve represents the attitudes adopting the transverse gallop gait. The green and brown curves represent the attitudes adopting the scaled (1/2 and 1/3, respectively) transverse gallop gait.

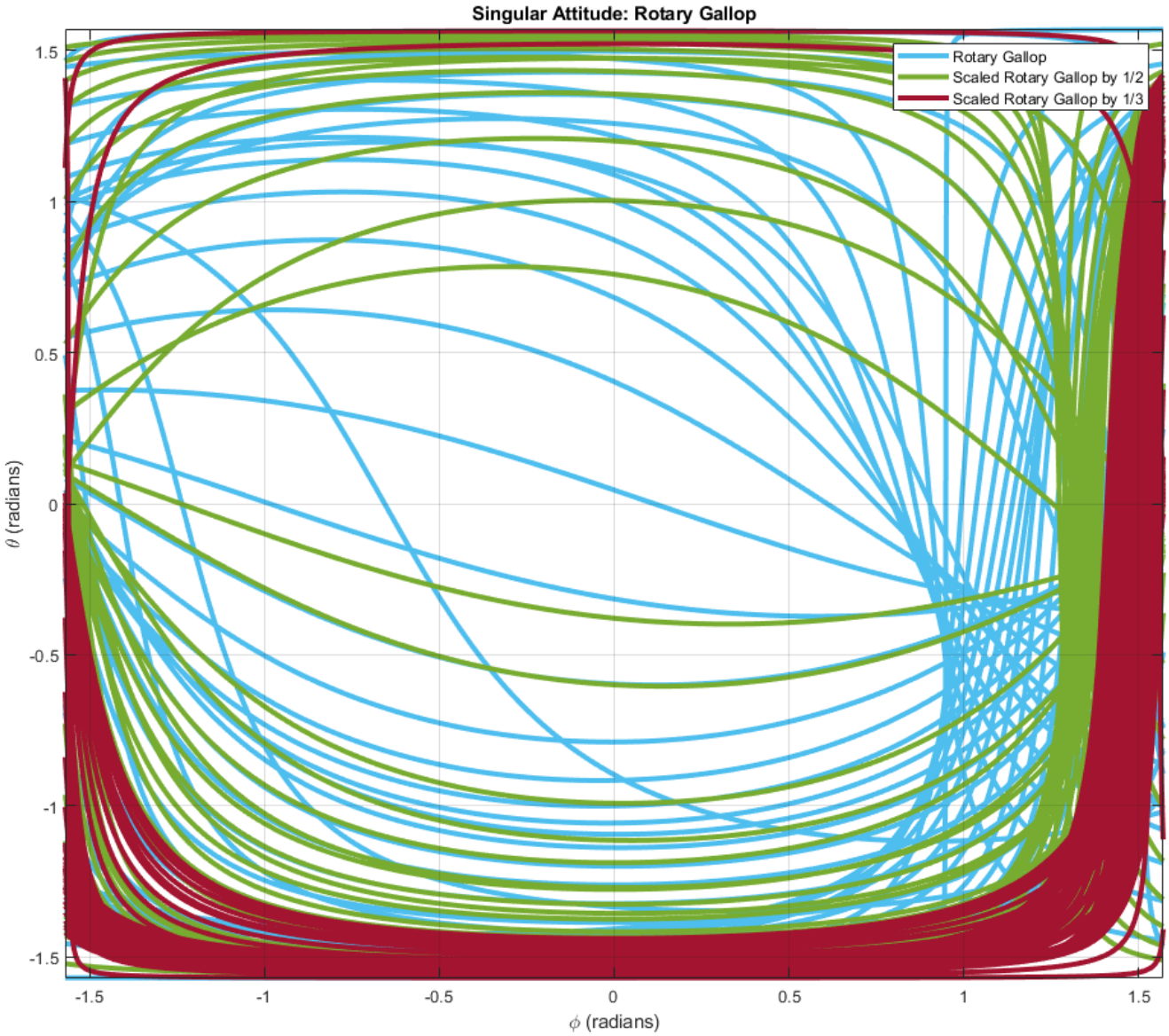

Figure 11. The attitudes introducing the singular decoupling matrix. The blue curve represents the attitudes adopting the rotary gallop gait. The green and brown curves represent the attitudes adopting the scaled (1/2 and 1/3, respectively) rotary gallop gait.

The unreferred gait, run gait, remains identical to the original cat-run gait.

5. Simulation Settings

Similar to our previous research [19], the references set in this research are the uniform rectilinear motion and the uniform circular motion with zero yaw and zero altitude ($\psi_r = 0, Z_r = 0$), which are specified as

$$\begin{cases} X_r = 1.5 \cdot t \\ Y_r = 1.5 \cdot t \end{cases}. \tag{19}$$

$$\begin{cases} X_r = 5 \cdot \cos(0.1 \cdot t) \\ Y_r = 5 \cdot \sin(0.1 \cdot t) \end{cases}. \tag{20}$$

We adopt this reference since this speed accommodates the cat-trot gait only, which is not preferable to any of the gaits analyzed in this study. The tilt-rotor is then required to track these unbiased references with the relevant gaits.

The absolute value of each initial angular velocity was 300 (rad/s). Each gait is adopted with three different periods (1 (s), 2 (s), and 3 (s)) to track these two references. In addition, the conventional attitude-position decoupler and the modified attitude-position decoupler for a tilt-rotor [19] are both tested and compared.

The supremum of the dynamic state error in position, after sufficient time, is defined as

$$\max_{t \geqslant 20s} \parallel e(t) \parallel \tag{21}$$

where $e(t)$ is the dynamic state error in position defined as

$$e = \sqrt{{e_X}^2 + {e_Y}^2} \tag{22}$$

where e_X and e_Y represent the dynamic state errors along X and Y directions, respectively.

The supremum of the dynamic state error in position, after sufficient time, is recorded and compared in each test.

The simulation is conducted in Simulink, MATLAB. Ode3 with sampling time 0.001 (s) is adopted in our solver.

6. Results

For the first reference, uniform rectilinear motion, the suprema of the dynamic state error (unit: meter), after sufficient time, for different gaits and different periods are concluded in Figure 12.

The results are classified into 3 sections based on the period of the gaits. They are 1 s (gray), 2 s (red), and 3 s (yellow), respectively. The axis W, R, TG, and RG represents walk gait, run gait, transverse gallop gait, and rotary gallop gait, respectively. The vertexes of the outer quadrilateral (blue) represent the result equipped with the conventional attitude-position decoupler. The vertexes of the inner quadrilateral (purple) represent the result equipped with the modified attitude-position decoupler, (12) and (13).

For example, the "2.47" on the "W" axis on the outer quadrilateral (blue) in "Period: 1 (s)" in Figure 12 means that the supremum of the dynamic state error, after sufficient time, is 2.47 m, adopting the walk-inspired gait with a period of 1 s equipped with the conventional attitude-position decoupler. The "0.19" on the "W" axis on the inner quadrilateral (purple) in "Period: 1 (s)" in Figure 12 means that the supremum of the dynamic state error, after sufficient time, is 0.19 m, adopting the walk-inspired gait with a period of 1 s equipped with the modified attitude-position decoupler.

In addition, the result of the simulation with the uniform circular motion is plotted in Figure 13.

The same notation rule is adopted. Specifically, the results are classified into 3 sections based on the period of the gaits. They are 1 s (gray), 2 s (red), and 3 s (yellow), respectively. The axis W, R, TG, and RG represents walk gait, run gait, transverse gallop gait, and rotary gallop gait, respectively. The vertexes of the outer quadrilateral (blue) represent the result equipped with the conventional attitude-position decoupler. The vertexes of the inner quadrilateral (purple) represents the result equipped with the modified attitude-position decoupler, (12) and (13).

It can be clearly seen that the inner purple quadrilateral is much smaller than the outer blue quadrilateral, which demonstrates that our modified attitude-position decoupler significantly decreases the dynamic state error for all the gaits discussed in this research. This novel attitude-position decoupler is particularly effective for the case suffering from a large dynamic state error equipped with the conventional attitude-position decoupler.

Another interesting result is that the choice of the period influences the dynamic state error. The longer the period is, the larger dynamic state error there tends to be in walk gait, run gait, transverse gallop gait, and rotary gallop gait. The result of the walk gaits is insignificantly influenced by the period settings, while the result in the run gait highly relies on the period settings.

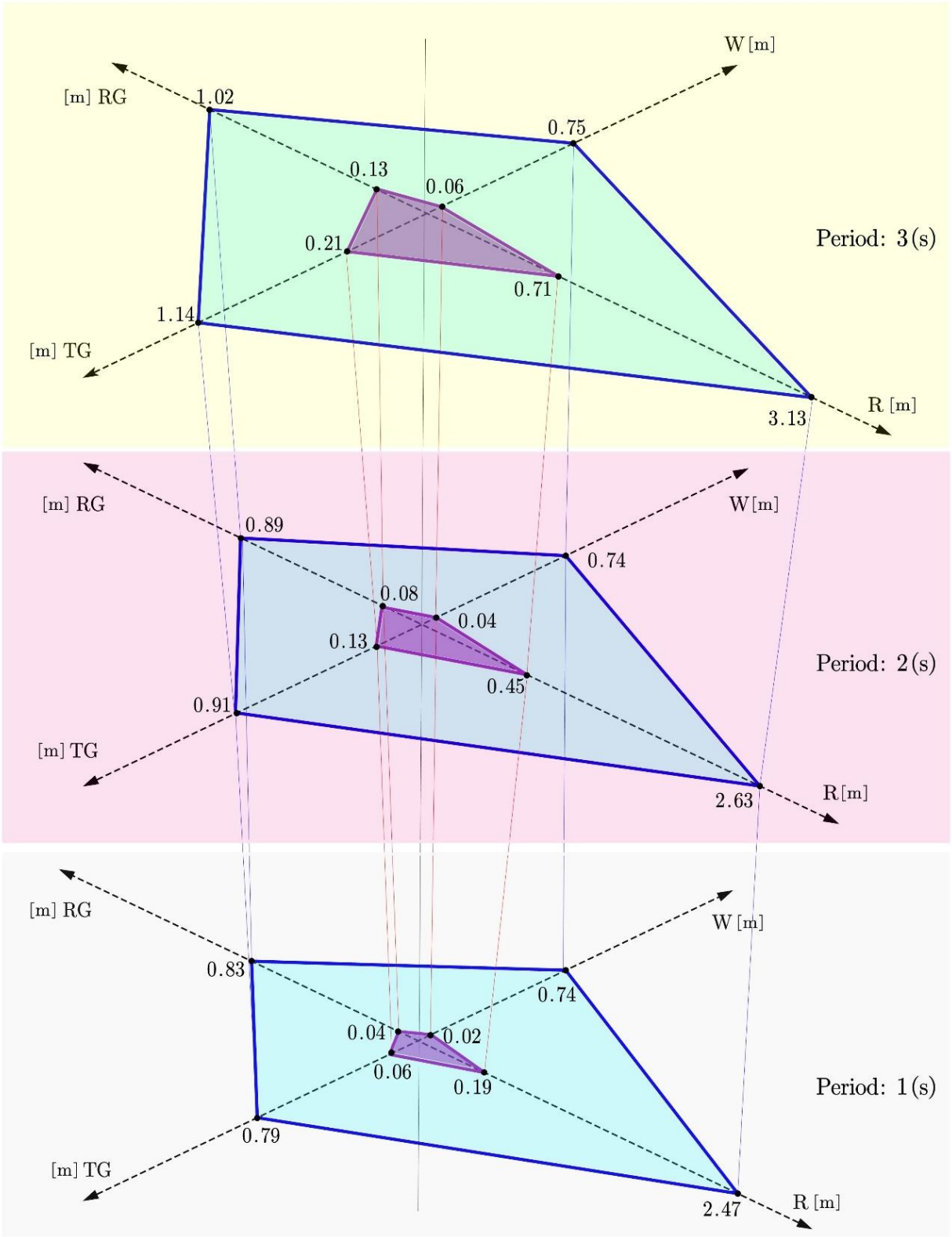

Figure 12. The result of the simulation with the uniform-rectilinear-motion reference: supremum of the dynamic state error (unit: m) after sufficient time for three different time periods. W: walk gait. R: run gait. TG: transverse gallop gait. RG: rotary gallop gait. Outer quadrilateral (blue): equip with the conventional attitude-position decoupler. Inner quadrilateral (purple): equip with the modified attitude-position decoupler.

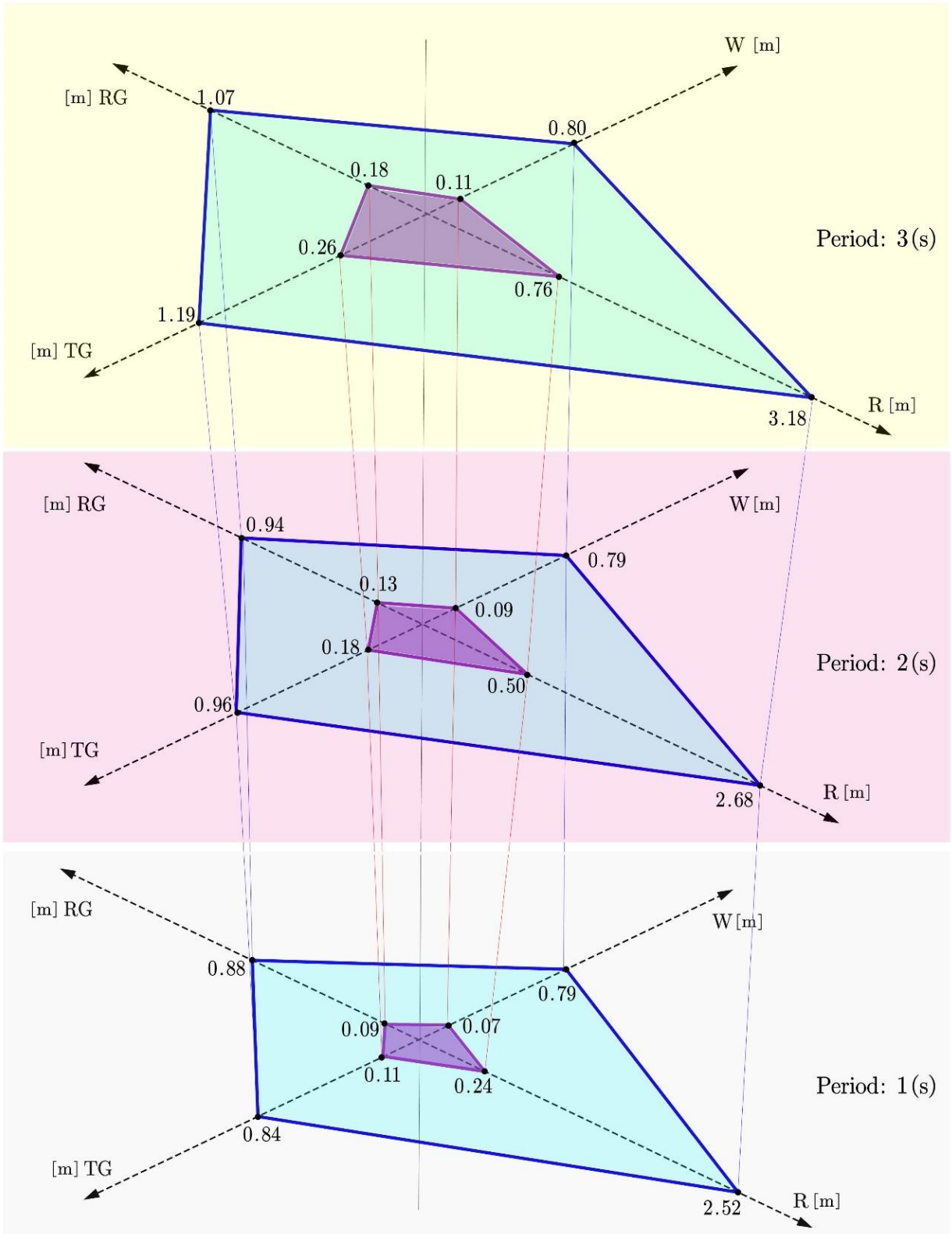

Figure 13. The result of the simulation with the uniform-circular-motion reference: supremum of the dynamic state error (unit: m) after sufficient time for three different time periods. W: walk gait. R: run gait. TG: transverse gallop gait. RG: rotary gallop gait. Outer quadrilateral (blue): equip with the conventional attitude-position decoupler. Inner quadrilateral (purple): equip with the modified attitude-position decoupler.

7. Conclusions and Discussions

The four cat gaits, walk gait, run gait, transverse gallop gait, and rotary gallop gait are feasible to be transplanted to solve the gait plan problem for a tilt-rotor. However, walk gait, transverse gallop gait, and rotary gallop gait are required to be modified, e.g., scaling, before being adopted.

The previous research proved that the cat-trot-gait planned tilt-rotor receives the invertible decoupling matrix near zero attitude region analytically. The parallel analytical necessary and sufficient condition to receive a regular decoupling matrix is not straightforward for the four cat gaits, walk gait, run gait, transverse gallop gait, and rotary gallop gait. Thus, this research proposed the singular curves in the roll-pitch diagram to analyze the property of the decoupling matrix for the first time.

Before this article, no systematic methods were put forward to modify a gait, which is liable to introduce a singular decoupling matrix in a tilt-rotor. The scaling method in the gait modification is proven to be feasible in finding a valid gait, liable to lead to the invertible decoupling matrix for the first time; this scaling method tends to enlarge the acceptable attitude zone in the roll-pitch diagram, indicating that this method strengthens the relevant gait.

The modified gaits in this simulation show promising tracking results, where the dynamic state error is acceptable in the tracking problem. Further, the modified walk-inspired gait in this research receives the least suprema of the dynamic state error after sufficient time, while the run-inspired gait receives the largest suprema of the dynamic state error after sufficient time. As for the rest of the gaits analyzed in his research, the modified transverse gallop gait and rotary gallop gait receive similar suprema of the dynamic state error after sufficient time. Beware that the dynamic state error may also be influenced by the maximum tilting angle of each gait, which is not identical in different gaits in this research.

It is not surprising that the modified attitude-position decoupler significantly reduces the dynamic state error for the tilt-rotor for each gait analyzed in this research; we have witnessed similar results in previous research [19]. This research further verifies the effectiveness of the modified attitude-position decoupler.

The length of the period of the gaits influences the dynamic state error. In general, the longer the period is, the larger dynamic state error there tends to be. Elucidating the underlying mechanism is beyond the scope of this research.

The unique contributions of this research can be concluded as follows: 1. A numerical method (singular curves in the roll-pitch diagram) of analyzing the robustness of the gaits is put forward for the first time. 2. A novel method for modifying the unqualified gaits is created and proven feasible theoretically. 3. The four typical cat-inspired gaits (walk gait, run gait, transverse gallop gait, and rotary gallop gait) are modified to accommodate the tracking problem based on feedback linearization.

Table 1 compares the methods in analyzing the property of the decoupling matrix of the animal-inspired gaits (cat walk/run/transverse gallop/rotary gallop) in this research and of the cat-trot inspired gait in the previous research.

Table 1. Methods in analyzing the property of the decoupling matrix.

Cat Trot	Cat Walk/Run/Transverse Gallop/Rotary Gallop
analytical conditions	numerical conditions
attitude is assumed zero	effects of the attitude are considered
-	put forward gait modification methods

There are several points worth exploring further. Firstly, since the scaling method is the only approach in modifying the gaits in this research, there might be other effective methods with sound mathematical grounds.

Figures 14 and 15 display the angular velocity histories while tracking the rectilinear reference defined in Formula (19) with the walk gait scaled by 1/3 and 1/6, respectively.

Though the periods of both gaits are identical (3 s), the scale of the tilting angles influences the resulting angular velocities of the propellers of the tilt-rotor. It can be asserted that the desired magnitude of the thrust of each propeller is influenced by the adopted gait.

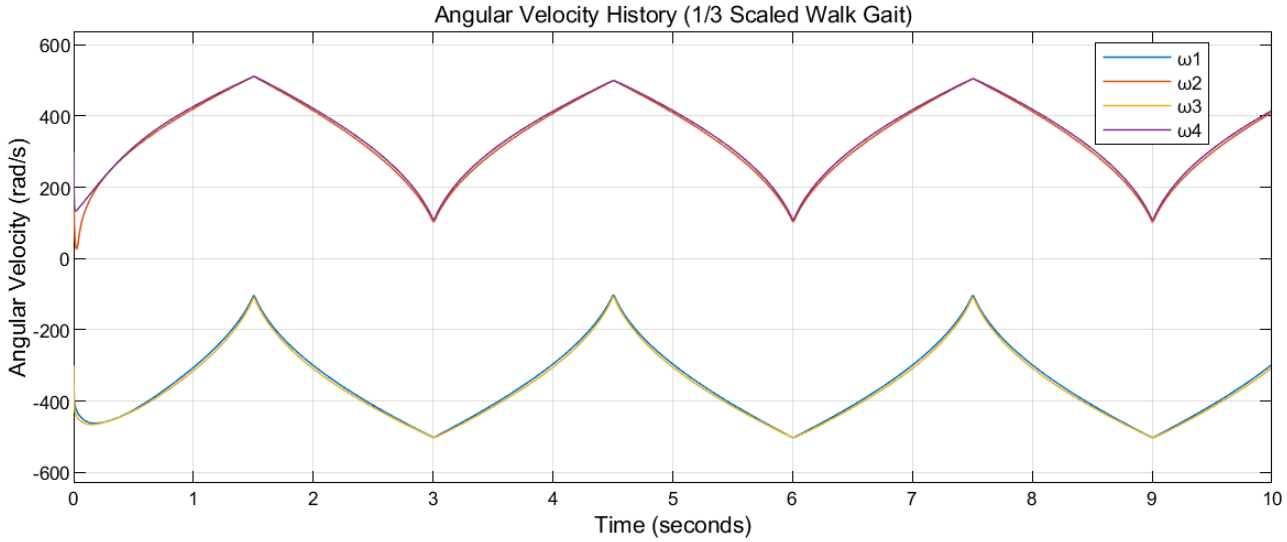

Figure 14. The angular velocities, ω_1, ω_2, ω_3, and ω_4, during the flight tracking the rectilinear reference. The scaled (1/3) walk gait is adopted with the period 3 s.

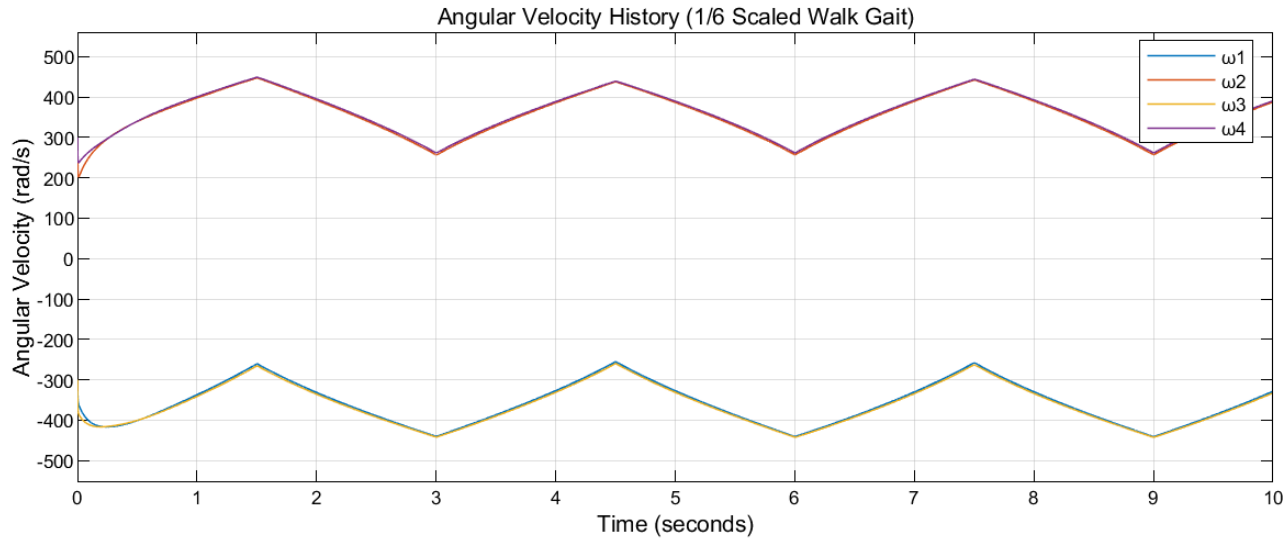

Figure 15. The angular velocities, ω_1, ω_2, ω_3, and ω_4, during the flight tracking the rectilinear reference. The scaled (1/6) walk gait is adopted with the period of 3 s.

It can also be found that the robustness of the tilt-rotor increases while scaling. This process, however, sacrifices the lateral force generated by the tilt-rotor. The trade-off between the scaling of the magnitude of the lateral force would be interesting to investigate during further research, as well as a real model to test this rule.

Author Contributions: Conceptualization, Z.S.; methodology, Z.S.; software, Z.S.; validation, Z.S.; formal analysis, Z.S.; investigation, Z.S.; resources, Z.S.; data curation, Z.S.; writing—original draft preparation, Z.S.; writing—review and editing, Z.S.; visualization, Z.S.; supervision, T.T.; project administration, T.T.; funding acquisition, T.T. All authors have read and agreed to the published version of the manuscript.

Funding: This research received no external funding.

Institutional Review Board Statement: Not applicable.

Informed Consent Statement: Not applicable.

Data Availability Statement: Not applicable.

Conflicts of Interest: The authors declare no conflict of interest.

Appendix A

This appendix details the PD controllers, $\begin{bmatrix} \dddot{y}_{1d} & \dddot{y}_{2d} & \dddot{y}_{3d} & \dddot{y}_{4d} \end{bmatrix}^T$, in (10) as follows

$$\begin{bmatrix} \dddot{y}_{1d} \\ \dddot{y}_{2d} \\ \dddot{y}_{3d} \\ \dddot{y}_{4d} \end{bmatrix} = \begin{bmatrix} \dddot{y}_{1r} \\ \dddot{y}_{2r} \\ \dddot{y}_{3r} \\ \dddot{y}_{4r} \end{bmatrix} + K_1 \cdot \left(\begin{bmatrix} \ddot{y}_{1r} \\ \ddot{y}_{2r} \\ \ddot{y}_{3r} \\ \ddot{y}_{4r} \end{bmatrix} - \begin{bmatrix} \ddot{y}_{1} \\ \ddot{y}_{2} \\ \ddot{y}_{3} \\ \ddot{y}_{4} \end{bmatrix} \right) + K_2 \cdot \left(\begin{bmatrix} \dot{y}_{1r} \\ \dot{y}_{2r} \\ \dot{y}_{3r} \\ \dot{y}_{4r} \end{bmatrix} - \begin{bmatrix} \dot{y}_{1} \\ \dot{y}_{2} \\ \dot{y}_{3} \\ \dot{y}_{4} \end{bmatrix} \right) + K_3 \cdot \left(\begin{bmatrix} y_{1r} \\ y_{2r} \\ y_{3r} \\ y_{4r} \end{bmatrix} - \begin{bmatrix} y_{1} \\ y_{2} \\ y_{3} \\ y_{4} \end{bmatrix} \right) \tag{A1}$$

where $y_{ir} (i = 1, 2, 3, 4)$ represents the reference which is defined in Section 5, K_1, K_2, and K_3 are the control coefficients,

$$K_1 = \begin{bmatrix} 1 & & & \\ & 1 & & \\ & & 1 & \\ & & & 10 \end{bmatrix}, \tag{A2}$$

$$K_2 = \begin{bmatrix} 10 & & & \\ & 10 & & \\ & & 1 & \\ & & & 5 \end{bmatrix}, \tag{A3}$$

$$K_3 = \begin{bmatrix} 50 & & & \\ & 50 & & \\ & & 1 & \\ & & & 10 \end{bmatrix}. \tag{A4}$$

The stability proof can be found by substituting (A1)–(A4) into (10).

References

1. Ryll, M.; Bulthoff, H.H.; Giordano, P.R. A novel overactuated quadrotor unmanned aerial vehicle: Modeling, control, and experimental validation. *IEEE Trans. Control Syst. Technol.* **2015**, *23*, 540–556. [CrossRef]
2. Jin, S.; Bak, J.; Kim, J.; Seo, T.; Kim, H.S. Switching PD-based sliding mode control for hovering of a tilting-thruster underwater robot. *PLoS ONE* **2018**, *13*, e0194427. [CrossRef] [PubMed]
3. Kumar, R.; Sridhar, S.; Cazaurang, F.; Cohen, K.; Kumar, M. *Reconfigurable Fault-Tolerant Tilt-Rotor Quadcopter System*; American Society of Mechanical Engineers: Atlanta, GA, USA, 2018; p. V003T37A008.
4. Anderson, R.B.; Marshall, J.A.; L'Afflitto, A. constrained robust model reference adaptive control of a tilt-rotor quadcopter pulling an unmodeled cart. *IEEE Trans. Aerosp. Electron. Syst.* **2021**, *57*, 39–54. [CrossRef]
5. Invernizzi, D.; Giurato, M.; Gattazzo, P.; Lovera, M. Comparison of control methods for trajectory tracking in fully actuated unmanned aerial vehicles. *IEEE Trans. Control Syst. Technol.* **2021**, *29*, 1147–1160. [CrossRef]
6. Invernizzi, D.; Lovera, M. Trajectory tracking control of thrust-vectoring UAVs. *Automatica* **2018**, *95*, 180–186. [CrossRef]
7. Imamura, A.; Miwa, M.; Hino, J. Flight characteristics of quad rotor helicopter with thrust vectoring equipment. *J. Robot. Mechatron.* **2016**, *28*, 334–342. [CrossRef]
8. Ryll, M.; Bulthoff, H.H.; Giordano, P.R. First flight tests for a quadrotor UAV with tilting propellers. In Proceedings of the 2013 IEEE International Conference on Robotics and Automation, Karlsruhe, Germany, 6–8 May 2013; IEEE: Karlsruhe, Germany, 2013; pp. 295–302.
9. Michieletto, G.; Cenedese, A.; Zaccarian, L.; Franchi, A. Hierarchical nonlinear control for multi-rotor asymptotic stabilization based on zero-moment direction. *Automatica* **2020**, *117*, 108991. [CrossRef]
10. Nemati, A.; Kumar, M. Modeling and control of a single axis tilting quadcopter. In Proceedings of the 2014 American Control Conference, Portland, OR, USA, 4–6 June 2014; IEEE: Portland, OR, USA; pp. 3077–3082.
11. Jin, S.; Kim, J.; Kim, J.-W.; Bae, J.; Bak, J.; Kim, J.; Seo, T. Back-stepping control design for an underwater robot with tilting thrusters. In Proceedings of the 2015 International Conference on Advanced Robotics (ICAR), Istanbul, Turkey, 27–31 July 2015; IEEE: Istanbul, Turkey; pp. 1–8.

12. Ryll, M.; Bulthoff, H.H.; Giordano, P.R. Modeling and control of a quadrotor UAV with tilting propellers. In Proceedings of the 2012 IEEE International Conference on Robotics and Automation, St Paul, MN, USA, 14–18 May 2012; IEEE: St Paul, MN, USA; pp. 4606–4613.
13. Shen, Z.; Ma, Y.; Tsuchiya, T. Stability analysis of a feedback-linearization-based controller with saturation: A tilt vehicle with the penguin-inspired gait plan. *arXiv* **2021**, arXiv:211114456.
14. Franchi, A.; Carli, R.; Bicego, D.; Ryll, M. Full-pose tracking control for aerial robotic systems with laterally bounded input force. *IEEE Trans. Robot.* **2018**, *34*, 534–541. [CrossRef]
15. Shen, Z.; Tsuchiya, T. State drift and gait plan in feedback linearization control of a tilt vehicle. In *Proceedings of the Computer Science & Information Technology (CS & IT), Vienna, Austria, 2022*; Academy & Industry Research Collaboration Center (AIRCC): Vienna, Austria, 2022; pp. 1–17.
16. Kumar, R.; Nemati, A.; Kumar, M.; Sharma, R.; Cohen, K.; Cazaurang, F. *Tilting-Rotor Quadcopter for Aggressive Flight Maneuvers Using Differential Flatness Based Flight Controller*; American Society of Mechanical Engineers: Tysons, VA, USA, 2017; p. V003T39A006.
17. Hamandi, M.; Usai, F.; Sablé, Q.; Staub, N.; Tognon, M.; Franchi, A. design of multirotor aerial vehicles: A taxonomy based on input allocation. *Int. J. Robot. Res.* **2021**, *40*, 1015–1044. [CrossRef]
18. Shen, Z.; Tsuchiya, T. Gait analysis for a tiltrotor: The dynamic invertible gait. *Robotics* **2022**, *11*, 33. [CrossRef]
19. Shen, Z.; Ma, Y.; Tsuchiya, T. Feedback linearization based tracking control of a tilt-rotor with cat-trot gait plan. *arXiv* **2022**, arXiv:2202.02926.
20. Vilensky, J.A.; Njock Libii, J.; Moore, A.M. Trot-gallop gait transitions in quadrupeds. *Physiol. Behav.* **1991**, *50*, 835–842. [CrossRef]
21. Luukkonen, T. Modelling and control of quadcopter. *Indep. Res. Proj. Appl. Math. Espoo* **2011**, *22*, 22.
22. Goodarzi, F.A.; Lee, D.; Lee, T. Geometric adaptive tracking control of a quadrotor unmanned aerial vehicle on SE(3) for agile maneuvers. *J. Dyn. Syst. Meas. Control* **2015**, *137*, 091007. [CrossRef]
23. Shi, X.-N.; Zhang, Y.-A.; Zhou, D. A geometric approach for quadrotor trajectory tracking control. *Int. J. Control* **2015**, *88*, 2217–2227. [CrossRef]
24. Lee, T.; Leok, M.; McClamroch, N.H. Nonlinear robust tracking control of a quadrotor UAV on SE(3): Nonlinear robust tracking control of a quadrotor UAV. *Asian J. Control* **2013**, *15*, 391–408. [CrossRef]
25. Rajappa, S.; Ryll, M.; Bulthoff, H.H.; Franchi, A. Modeling, control and design optimization for a fully-actuated hexarotor aerial vehicle with tilted propellers. In Proceedings of the 2015 IEEE International Conference on Robotics and Automation (ICRA), Seattle, WA, USA, 26–30 May 2015; IEEE: Seattle, WA, USA; pp. 4006–4013.
26. Ansari, U.; Bajodah, A.H.; Hamayun, M.T. Quadrotor control via robust generalized dynamic inversion and adaptive non-Singular terminal sliding mode. *Asian J. Control* **2019**, *21*, 1237–1249. [CrossRef]
27. Kolmanovsky, I.; Kalabić, U.; Gilbert, E. Developments in constrained control using reference governors. *IFAC Proc. Vol.* **2012**, *45*, 282–290. [CrossRef]